

Electronic Supplementary Information

Copper-Modulated Nanocrystal Bismuth Alters Formate Formation Pathway to Achieve Highly Selective CO₂ Electroreduction

Meng Yang Zu,^a Le Zhang,^a Chongwu Wang,^a Li Rong Zheng^b and Hua Gui Yang^{*a}

^a Key Laboratory for Ultrafine Materials of Ministry of Education, School of Materials Science and Engineering, East China University of Science and Technology, Shanghai, 200237 (China)

^b Beijing Synchrotron Radiation Facility, Institute of High Energy Physics, Chinese Academy of Sciences, Beijing, 100049 (China)

* Corresponding author: hgyang@ecust.edu.cn (H. G. Y).

Experimental Section

Chemicals. Bismuth iodide (BiI_3), copper(II) acetylacetonate $\text{Cu}(\text{acac})_2$, oleylamine, 1-octadecene, ascorbic acid (L-AA) and Nafion (5 wt%) were obtained from Sigma-Aldrich. Carbon black (Vulcan XC72R) was purchased from Carbot Corp. Potassium bicarbonate (KHCO_3), nitric acid (HNO_3) and isopropanol were purchased from Shanghai Chemical Reagent Co. Ltd. All chemicals were of analytical grade and used without any further purification. Toray carbon paper (1 cm * 2 cm) was pre-treated in boiling HNO_3 for 12 h at the temperature of 100 °C. Argon (Ar, 99.99%) and carbon dioxide (CO_2 , 99.9999%) were purchased from Shanghai Haizhou Special Gas Co., Ltd.

Preparation of Catalysts. In a typical synthesis of CuBi catalyst, 0.2 mmol $\text{Cu}(\text{acac})_2$, 0.2 mmol BiI_3 and 200mg L-AA were dissolved in a mixed solution of 8 mL 1-octadecene and 2 mL oleylamine, and then the above mixture was transferred into a 25 mL, three-necked, round-bottomed flask. Followed by stirring under vacuum at 80 °C for 10 min, the reaction was placed under Ar and heated from 80 to 200 °C in 10 min, and then was maintained at 200 °C for 1 h. After cooling down to room temperature, the product was centrifuged at 10000 rpm for 5 min in hexane for several times, and then dried overnight in vacuum at 60 °C. For bare nanocrystal Bi catalyst, the synthesis process is similar except for that 0.4 mmol BiI_3 was added and no addition of $\text{Cu}(\text{acac})_2$. Likewise, for bare Cu catalyst, the synthesis process is similar except for that 0.4 $\text{Cu}(\text{acac})_2$ was added and no addition of BiI_3 . In addition, for 0.5-CuBi and 2.0-CuBi samples, the synthesis process is similar except for that 0.1 mmol and 0.4 mmol $\text{Cu}(\text{acac})_2$ was added into 0.2 mmol BiI_3 , respectively.

Electrochemical measurements. Electrochemical measurements were performed by using a Model CHI 660E potentiostat in a two-compartment electrochemical cell, and Nafion 115, which is a proton exchange membrane, was used to separate the catholyte and the anolyte. To prepare the working electrode, 10 mg catalyst (CuBi or Bi), 10 mg carbon black and 80 μL Nafion solution (5 wt%) were dispersed in 1 mL isopropanol by at least 30 min sonication to form a homogeneous ink, followed by dipping the ink on the pre-treated carbon paper (geometric area of 1 cm^2 and mass loading of the catalyst is 2 mg cm^{-2}). Ag/AgCl (3.5 M KCl) and gauze platinum were used as the reference electrode and the counter electrode, respectively. The electrocatalytic tests of the catalysts were examined by polarization curves with a scan rate of 5 mV s^{-1} in the CO_2 or Ar saturated 0.5 M KHCO_3 at room temperature. All potentials were referenced to reversible

hydrogen electrode (RHE) by following calculations: $E_{\text{RHE}} = E_{\text{Ag/AgCl}} + 0.059 \times \text{pH} + 0.205$. AC impedance measurements were carried out in the same configuration when the working electrode was biased at a certain overpotential from 10^5 Hz to 0.1 Hz with an AC voltage of 5 mV. The CO_2 reduction reaction was measured by using chronoamperometry at each fixed potential and gaseous products (i.e., H_2 and CO) were quantified using a gas chromatography (GC) system (RAMIN, GC2060) that was equipped with a flame ionization detector (FID) and a thermal conductivity detector (TCD). Ultrahigh purity argon gas (Ar, 99.99%) was used as the carrier gas. The average CO_2 flow rate was 5 sccm, which was measured by a universal flow meter (Alicat Scientific, LK2) at the entrance of the electrochemical cell.

The Faradaic efficiency (FE) for formation of H_2 or CO was calculated as below:

$$FE = 2FvGP / RTi \times 100\%$$

v (vol%) is the volume concentration of H_2 in the exhaust gas from the electrochemical cell (GC data). G (mL min^{-1} at room temperature and ambient pressure) is the gas flow rate. i (mA) is the steady-state cell current. $P = 1.01 \times 10^5$ Pa, $T = 273.15$ K, $F = 96485$ C mol^{-1} , $R = 8.314$ J mol^{-1} K^{-1} .

Liquid product of HCOOH was quantified using ^1H nuclear magnetic resonance (NMR). For analysis, a 0.5 ml aliquot of the electrolyte was mixed with 0.1 ml D_2O (with TMS as the internal standard). The ^1H spectrum was measured with water suppression using a pre-saturation method.

We should note that conducting electrochemical experiments under an Ar atmosphere yielded only H_2 at all tested voltages, no hydrocarbons or CO could be detected *via* GC analysis.

Characterizations. The crystal structure was determined using X-ray diffraction (Bruker D8 Advanced Diffractometer with $\text{Cu K}\alpha$ radiation). The morphologies of the catalysts were examined by scanning electron microscope (Hitachi S4800) and transmission electron microscope (JEM 2100, 200 kV). Furthermore, the chemical states of the elements in catalysts were studied by X-ray photoelectron spectroscopy (Kratos Axis Ultra DLD), and the binding energy of the C 1s peak at 284.8 eV was taken as an internal reference. Bi L-edge X-ray absorption fine structure was performed on the 1W1B beamline of the Beijing Synchrotron Radiation Facility, China, operated at ~ 200 mA and ~ 2.5 GeV.

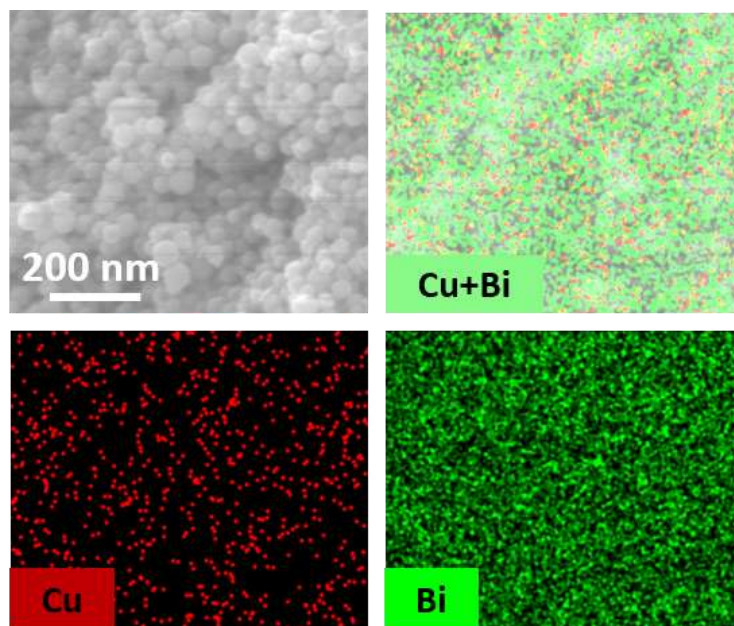


Fig. S1 SEM image and corresponding elemental mappings of CuBi, revealing the uniform distribution of Cu and Bi elements on CuBi nanoparticles.

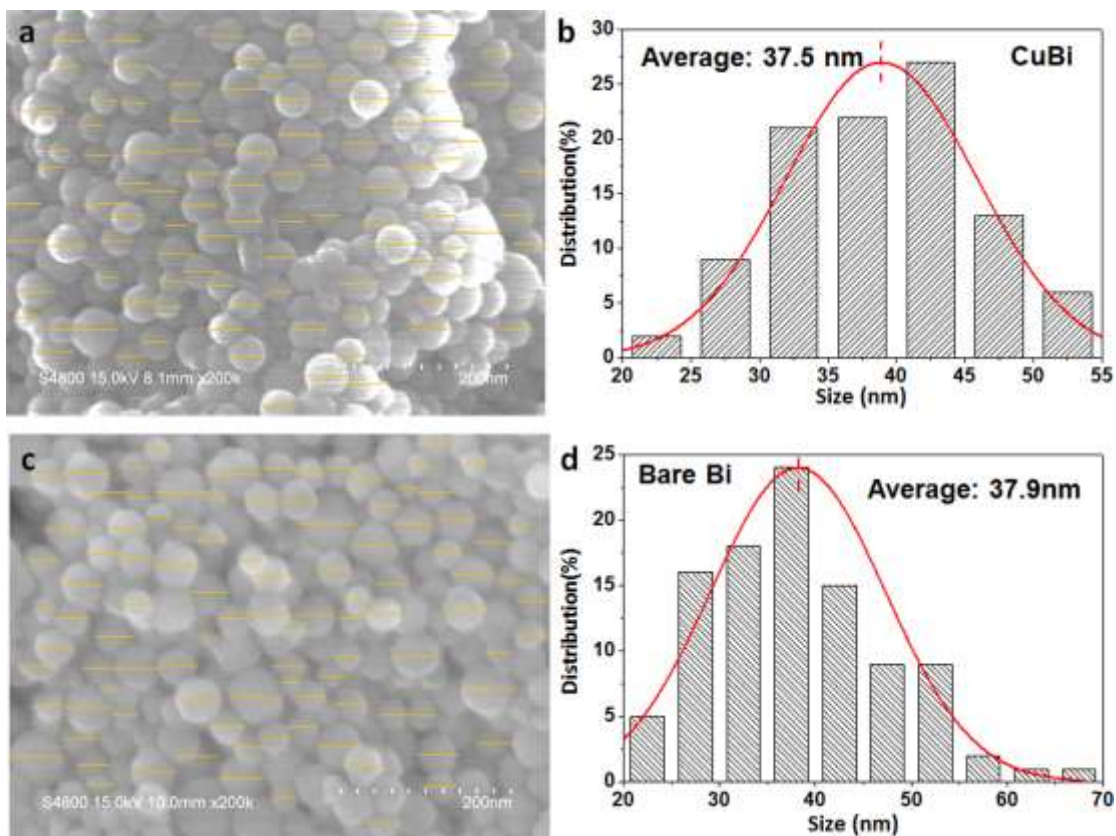


Fig. S2 SEM image of (a) CuBi and (c) bare Bi catalysts with a suitable field of view to show sufficient amount of nanoparticles. Particle size distribution histograms and lognormal fittings for the nanoparticles counted in the left SEM image, revealing an average particle size of 37.5 and 37.9 nm for (b) CuBi and (d) bare Bi catalysts, respectively.

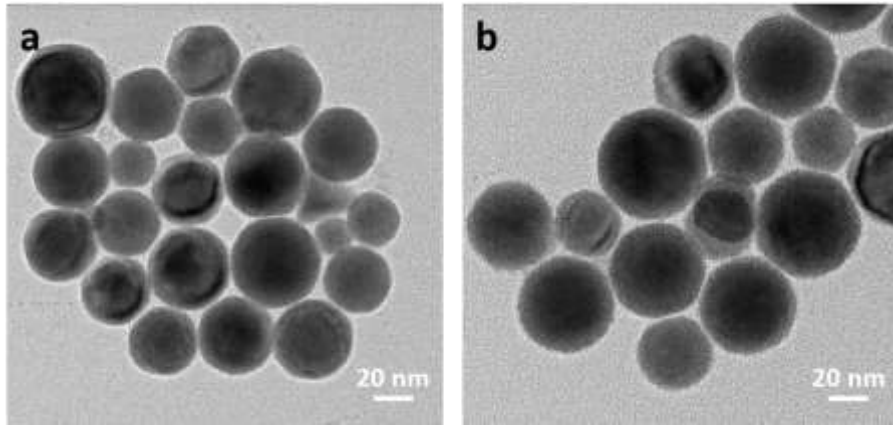


Fig. S3 TEM images of (a) CuBi and (b) bare Bi nanoparticles, displaying the similar morphologies as the SEM images.

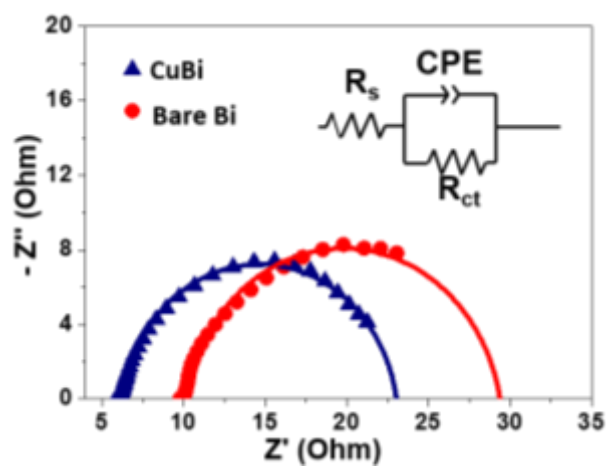


Fig. S4 Nyquist plots for CO₂RR for the samples of CuBi and bare Bi, and the inset of Figure 22 is the equivalent circuit used for fitting the Nyquist plots.

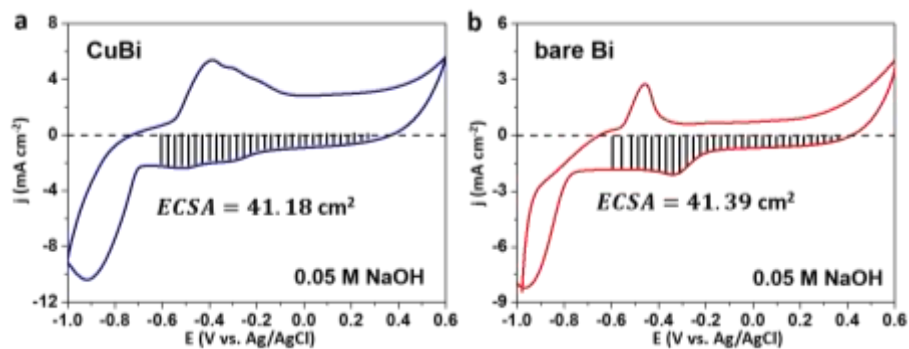


Fig. S5 ECSA for (a) CuBi and (b) bare Bi catalyst calculated by cyclic voltammograms (scanning direction: $-1.0 \rightarrow 0.6 \rightarrow -1.0$ V) in 0.05 M NaOH. The electrode has a 1 cm² exposed area. The results show that CuBi and bare Bi catalyst possessing ECSAs of 41.18 and 41.39 cm², respectively.

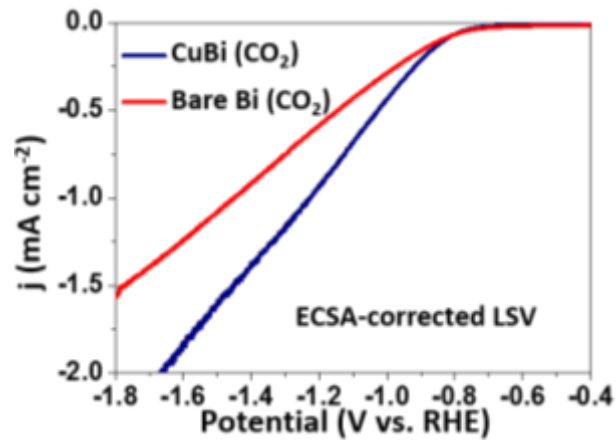


Fig. S6 ECSA-corrected LSV curves for CuBi and bare Bi catalysts in CO₂-saturated electrolyte. The current densities for CuBi catalyst are still higher than bare Bi catalyst after ECSA-correction, excluding the influence from morphology effects.

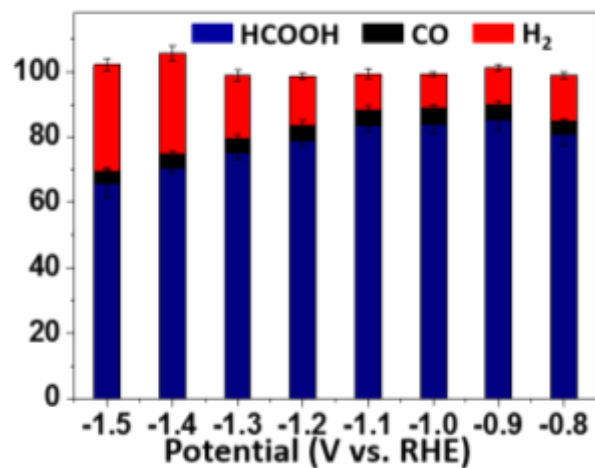


Fig. S7 Faradaic efficiencies of HCOOH, CO and H₂ for bare Bi. The FE_{HCOOH} decreased and the FE_{H₂} increased gradually with the potential rising, and this trend is in agreement with the scaling relation between the binding affinities for COOH* and H* *via* the pathway 1.

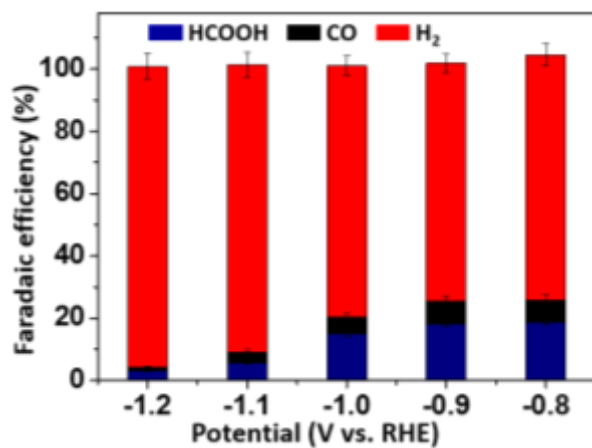


Fig. S8. Faradaic efficiencies of HCOOH, CO and H₂ for the bare Cu sample, and the main product is H₂.

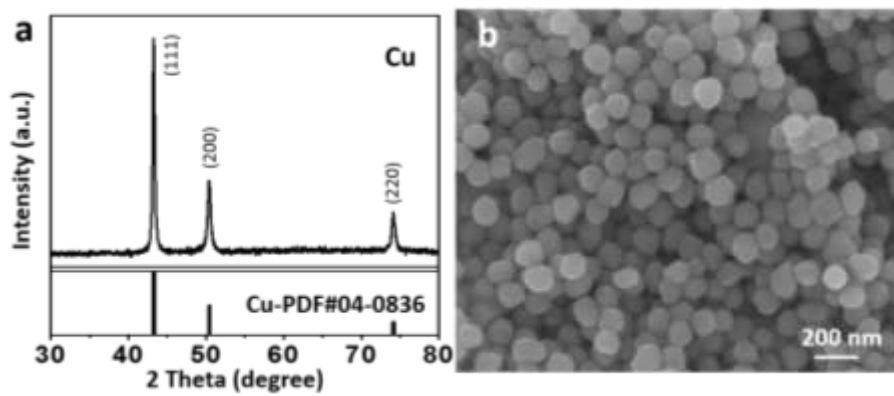


Fig. S9. XRD pattern and SEM image of bare Cu catalyst, illustrating the similar morphology as bare Bi and CuBi samples.

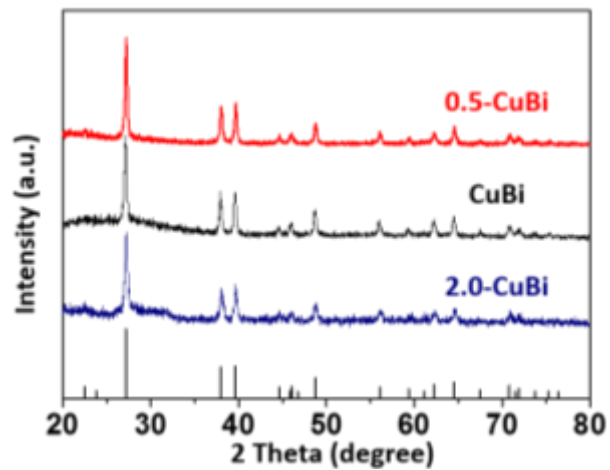


Fig. S10. XRD patterns of CuBi, 0.5-CuBi and 2.0-CuBi samples, demonstrating that the crystal structures of 0.5-CuBi and 2.0-CuBi samples are the same as CuBi, and exhibiting the crystalline phase of standard Bi.

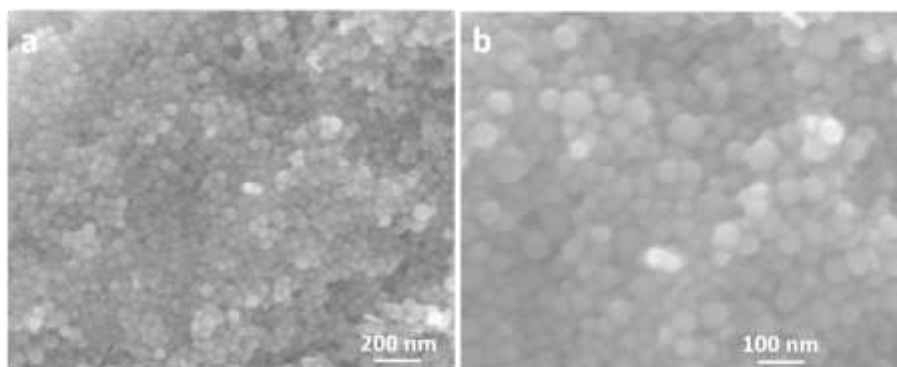


Fig. S11. SEM images of 0.5-CuBi at different magnifications, illustrating the similar morphologies of CuBi and bare Bi catalysts.

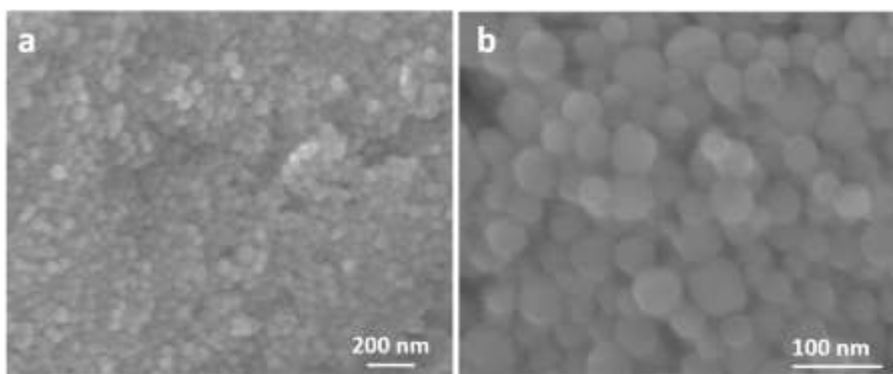


Fig. S12. SEM images of 2.0-CuBi at different magnifications, illustrating the similar morphologies of CuBi and bare Bi catalysts.

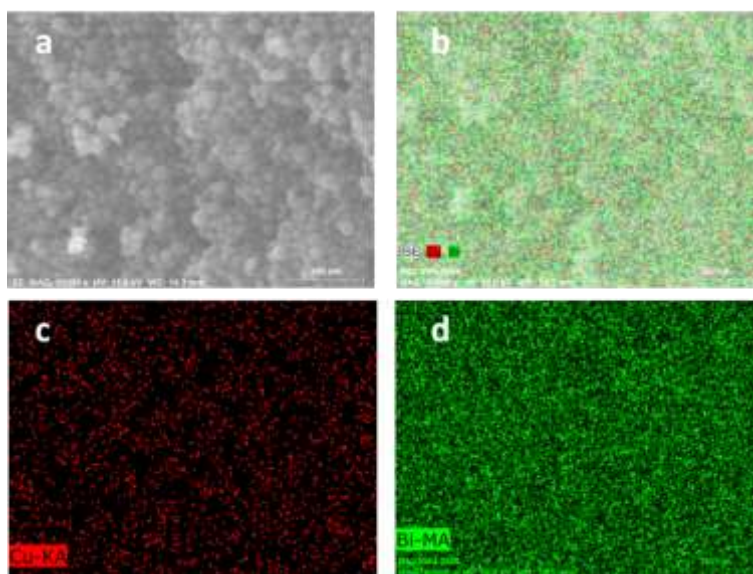


Fig. S13. SEM image and corresponding elemental mappings of 0.5-CuBi, revealing the uniform distribution of Cu and Bi elements on 0.5-CuBi nanoparticles.

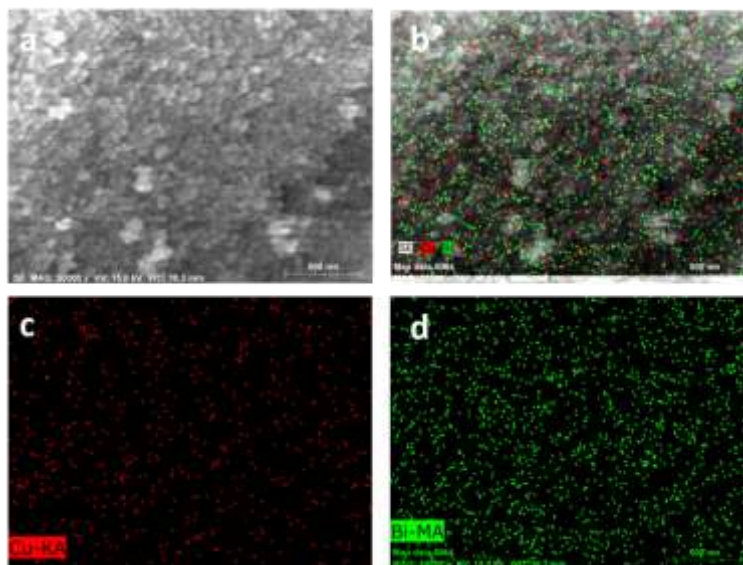


Fig. S14. SEM image and corresponding elemental mappings of 2.0-CuBi, revealing the uniform distribution of Cu and Bi elements on 2.0-CuBi nanoparticles.

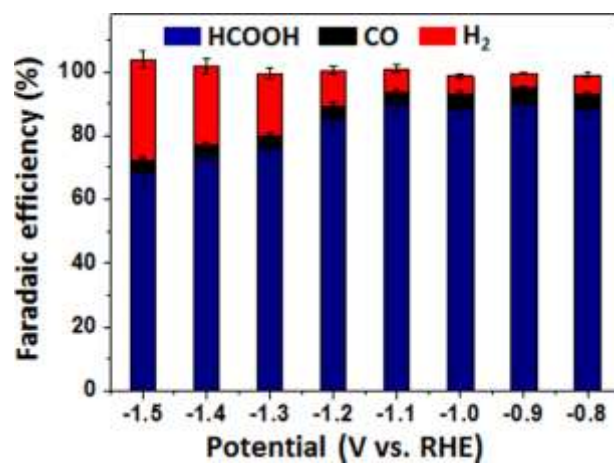


Fig. S15. Faradaic efficiencies of HCOOH, CO and H₂ for the sample 0.5-CuBi.

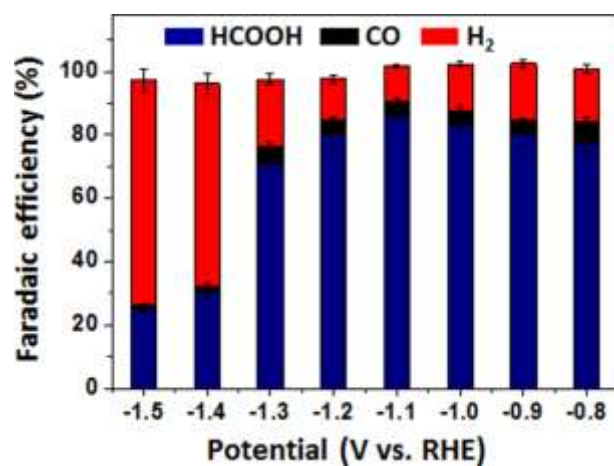


Fig. S16. Faradaic efficiencies of HCOOH, CO and H₂ for the sample 2.0-CuBi.

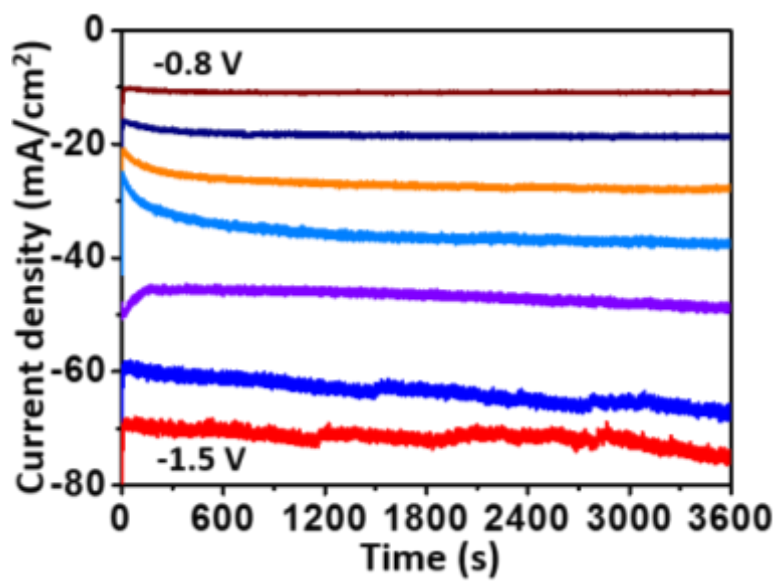


Fig. S17. Chronoamperometric curves of CuBi at different potentials from -0.8 to -1.5 V for continuous CO₂RR process in CO₂ saturated 0.5 M KHCO₃.

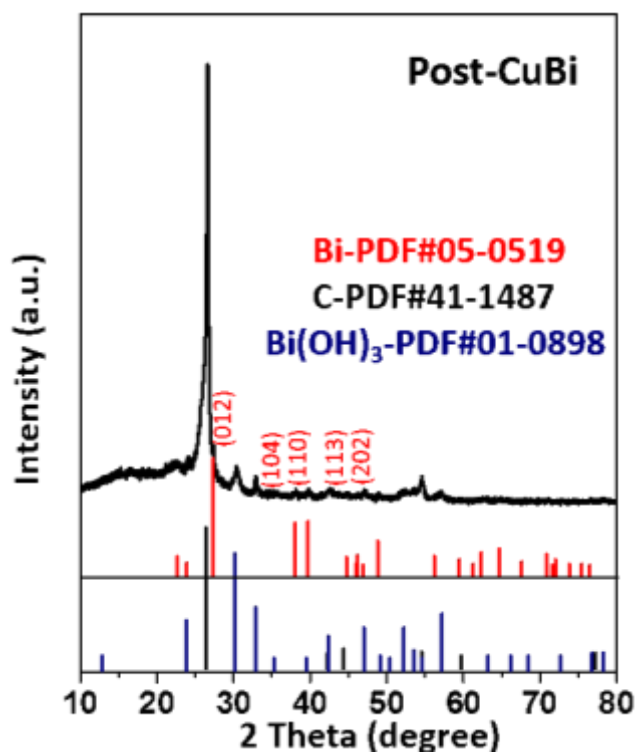


Fig. S18. XRD patterns of post-CuBi sample, demonstrating that the material consists of original metallic Bi, newly generated Bi(OH)₃ and carbon (mainly from the carbon paper substrate and carbon black).

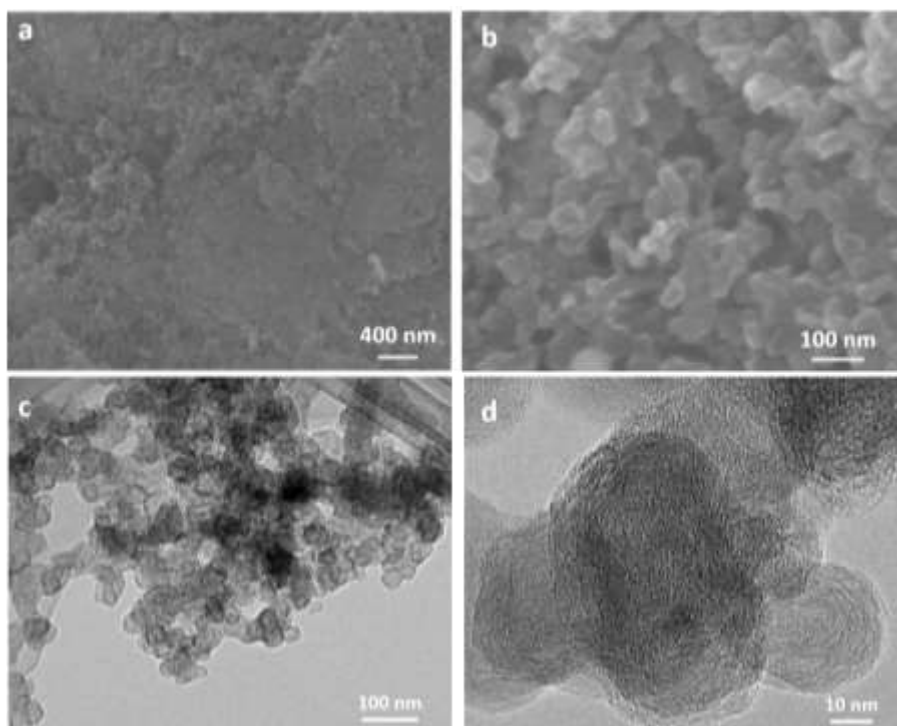


Fig. S19. (a, b) SEM and (c, d) TEM images of post-CuBi sample at different magnifications, displaying the similar morphologies of small nanoparticles with an average of 30-40 nm as original CuBi catalyst. Additionally, the small nanoparticles are surrounded by carbon black used to help the film formation on carbon paper substrate.

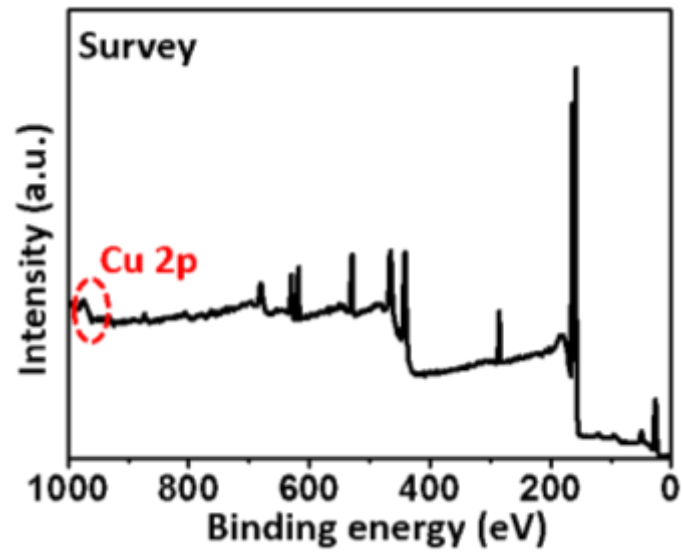


Fig. S20. XPS survey full scan of post-CuBi sample, indicating the existence of Cu element (dotted circle).

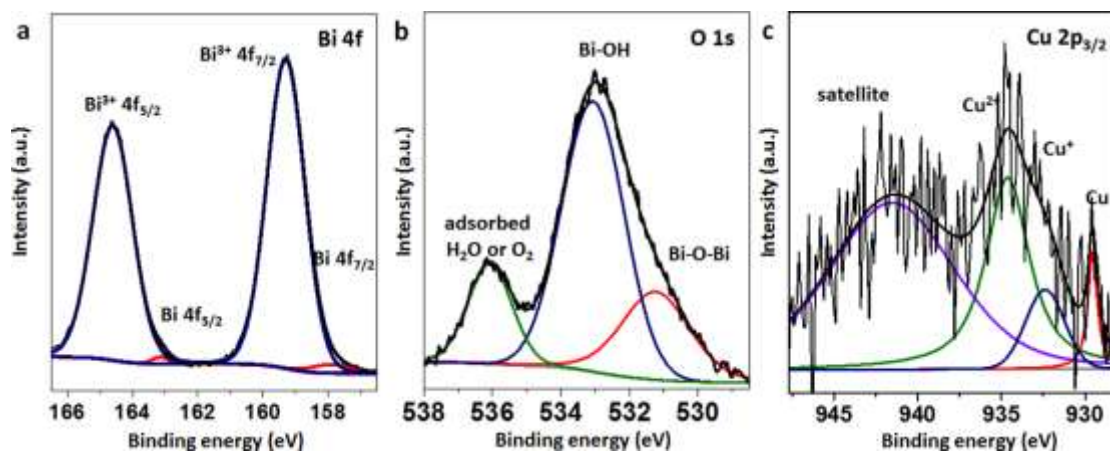


Fig. S21. XPS high-resolution spectra of (a) Bi 4f, (b) O 1s and (c) Cu 2p region for post-CuBi catalyst.

Element	Cu	Bi
Concentration (mg/L)	0.13	62
Molar concentration (mol/L)	2.05×10^{-3}	2.967×10^{-2}
Ratio of Cu:Bi	1:145	

Table S1. ICP-OES results of CuBi catalyst, illustrating the ratio of Cu:Bi for CuBi nanocrystals is 1:145.

Element	Title	Atomic (%)
C	C 1s	53.64
O	O 1s	28.83
Cu	Cu 2p	1.42
Bi	Bi 4f	16.11
Ratio of Cu:Bi	1:113	

Table S2. The peak table of XPS for CuBi sample, illustrating the ratio of Cu:Bi for CuBi nanocrystals is 1:113.

Element	Series	Atomic (%)
Cu	K-Series	0.86
Bi	M-Series	99.14
Ratio of Cu:Bi	1:115	

Table S3. The results of SEM-EDS for CuBi sample, illustrating the ratio of Cu:Bi for CuBi nanocrystals is 1:115.

Sample	R_s (Ω)	R_{ct} (Ω)
CuBi	6.30	17.98
Bare Bi	10.14	18.43

Table S4. The results of the fitted data obtained from equivalent circuit used for the Nyquist plots for CuBi and bare Bi catalysts. The R_s for CuBi and bare Bi catalysts are 6.30 and 10.14 Ω, respectively, illustrating that CuBi possesses better conductivity than bare Bi. The R_{ct} for CuBi and bare Bi catalysts are 17.89 and 18.43 Ω, respectively, which is quite close to each other.

Element	Title	Atomic (%)
Cu	Cu 2p	0.23
Bi	Bi 4f	2.46
Ratio of Cu:Bi	1:107	

Table S5. The peak table of XPS for CuBi sample after stability test, illustrating the ratio of Cu:Bi for post-CuBi sample is 1:107, which is pretty similar like original CuBi catalyst with a Cu:Bi ratio of 1:113.